



Tumor-immune microenvironment revealed by Imaging Mass Cytometry in a metastatic sarcomatoid urothelial carcinoma with a prolonged response to pembrolizumab

Hussein Alnajar,^{1,8} Hiranmayi Ravichandran,^{2,3,8} André Figueiredo Rendeiro,^{2,4} Kentaro Ohara,^{1,2} Wael Al Zoughbi,^{1,2} Jyothi Manohar,² Noah Greco,² Michael Sigouros,² Jesse Fox,⁵ Emily Muth,⁵ Samuel Angiuoli,⁵ Bishoy Faltas,^{2,6} Michael Shusterman,^{6,7} Cora N. Sternberg,^{2,6} Olivier Elemento,^{2,3,4} and Juan Miguel Mosquera^{1,2}

¹Department of Pathology and Laboratory Medicine, Weill Cornell Medicine, New York, New York, 10021, USA; ²Caryl and Israel Englander Institute for Precision Medicine, Weill Cornell Medicine and New York-Presbyterian, New York, New York 10021, USA; ³Department of Physiology and Biophysics, ⁴Institute for Computational Biomedicine, Weill Cornell Medicine, New York, New York, 10021, USA; ⁵Personal Genome Diagnostics, Inc., Baltimore, Maryland 21224, USA; ⁶Department of Medicine, Division of Hematology and Oncology, Weill Cornell Medicine, New York, New York 10021, USA

Abstract Sarcomatoid urothelial carcinoma (SUC) is a rare subtype of urothelial carcinoma (UC) that typically presents at an advanced stage compared to more common variants of UC. Locally advanced and metastatic UC have a poor long-term survival following progression on first-line platinum-based chemotherapy. Antibodies directed against the programmed cell death 1 protein (PD-1) or its ligand (PD-L1) are now approved to be used in these scenarios. The need for reliable biomarkers for treatment stratification is still under research. Here, we present a novel case report of the first Imaging Mass Cytometry (IMC) analysis done in SUC to investigate the immune cell repertoire and PD-L1 expression in a patient who presented with metastatic SUC and experienced a prolonged response to the anti-PD1 immune checkpoint inhibitor pembrolizumab after progression on first-line chemotherapy. This case report provides an important platform for translating these findings to a larger cohort of UC and UC variants.

Corresponding author:
jmm9018@med.cornell.edu

© 2022 Alnajar et al. This article is distributed under the terms of the Creative Commons Attribution-NonCommercial License, which permits reuse and redistribution, except for commercial purposes, provided that the original author and source are credited.

Ontology term: neoplasm of the genitourinary tract

Published by Cold Spring Harbor Laboratory Press

doi:10.1101/mcs.a006151

[Supplemental material is available for this article.]

INTRODUCTION

Urothelial carcinoma (UC) is a highly immunogenic malignancy (Gakis 2014). Intravesical bacillus Calmette–Guerin (BCG) therapy has been used in non-muscle-invasive bladder cancer over the last 40 years (Tripathi and Plimack 2018). Studies have demonstrated that UC has a high overall mutational burden, triggering an immune response, and tumor-associated

⁷Present address: NYU Langone Health, Perlmutter Cancer Center at NYU Langone Oncology & Hematology Associates, Mineola, New York 11501, USA

⁸Denotes co-first author.

lymphocytic infiltration (Tripathi and Plimack 2018). Programmed death-ligand-1 (PD-L1), also known as cluster of differentiation 274 (CD274), is an immunoinhibitory molecule mainly expressed on the surface of tumor cells and antigen-presenting cells in various solid malignancies that suppresses the activation of cytotoxic T cells, leading to tumor progression. Overexpression of PD-L1 in UC is associated with poor clinical outcomes, supporting the rationale for immune checkpoint blockade in advanced UC (Nakanishi et al. 2007).

Locally advanced and metastatic UC is an aggressive disease with poor long-term survival following progression on first-line platinum-based chemotherapy (De Santis et al. 2012). Recently, two antibodies directed against the programmed cell death 1 protein (PD-1) or its ligand (PD-L1) have been approved by the U.S. Food and Drug Administration for patients with advanced or metastatic UC who are ineligible to receive cisplatin-based chemotherapy and have a tumor expressing PD-L1 (pembrolizumab and atezolizumab). Five antibodies directed against the protein PD-1 or its ligand PD-L1 have been approved in patients who progress on or after a platinum-based chemotherapy. Two have recently been withdrawn from the U.S. market based on nonconfirmatory phase III studies (atezolizumab and durvalumab). However, many patients who receive checkpoint inhibitors do not achieve durable disease, and there is a need for reliable biomarkers for treatment stratification. Subgroup analyses of the KEYNOTE-045 trial showed continued clinical benefit of the anti-PD1 inhibitor pembrolizumab as second-line therapy in advanced/metastatic, platinum-refractory UC (Powles et al. 2020) over chemotherapy for efficacy and safety for treatment of locally advanced disease (Fradet et al. 2019). In KEYNOTE-045, PD-L1 was not significantly associated with improved outcomes of pembrolizumab or chemotherapy. Other recently identified potential biomarkers include tumor-infiltrating lymphocytes (TILs), microsatellite instability (MSI), tumor mutational burden (TMB), and the gut microbiome.

Sarcomatoid urothelial carcinoma (SUC) is a rare subtype of UC, with an incidence of 0.1%–0.3% across all bladder histologies (Cheng et al. 2011), whereas sarcomatoid features occur in up to 6% of UC cases. SUC typically presents at an advanced stage compared to more common variants of UC (stage T3-4, 34% vs. 28%) and is frequently associated with node-positive or metastatic disease (20% vs. 10%) (Wright et al. 2007). A retrospective analysis of 221 cases of SUC found that only 54% of patients were alive 1 year after cancer-directed surgery (Wang et al. 2010). No prospective data is available to guide management, and treatment is based on extrapolation from standard UC management (Grossman et al. 2003; Sternberg et al. 2006).

In this molecular case report, we present a patient with metastatic SUC, which demonstrated PD-L1 overexpression and gene amplification, who experienced a durable significant response to pembrolizumab. We demonstrate the combination of tissue- and plasma-based next-generation sequencing (NGS) complemented by Imaging Mass Cytometry (IMC) analysis (Giesen et al. 2014) of tissue to explore the immune cell repertoire.

RESULTS

Case Presentation

A 62-yr-old female with no significant comorbidities presented in February 2018 with hematuria. Cystoscopy revealed a noninvasive high-grade papillary urothelial carcinoma. The patient was lost to follow-up until January 2019 when she returned with difficulty voiding, pelvic pain, and gross hematuria. Cystoscopy revealed a large, organized clot in the bladder, and a computed tomography (CT) demonstrated an enhancing bladder tumor. Transurethral resection of the bladder tumor and fulguration was not successful, and the patient underwent a radical cystectomy, hysterectomy and bilateral salpingo-oophorectomy, anterior

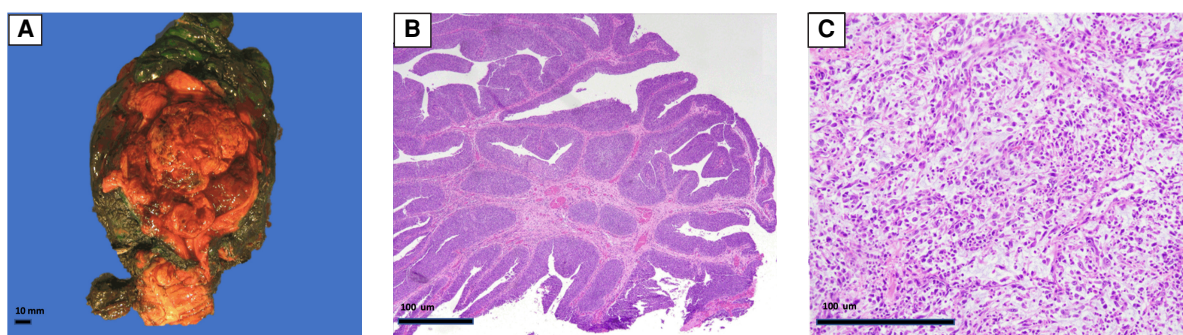


Figure 1. Histopathology of primary sarcomatoid urothelial carcinoma (UC) case. A radical cystectomy, hysterectomy and bilateral salpingo-oophorectomy, anterior vaginectomy showed a 6.5-cm bladder mass (A) with papillary high-grade urothelial carcinoma component (B) and an invasive malignant spindle cell component (C) diagnostic of sarcomatoid differentiation.

vaginectomy with pelvic lymph node dissection, and creation of a continent cutaneous urinary diversion (Fig. 1A). Pathology revealed a 6.5-cm high-grade urothelial carcinoma (Fig. 1B) with a malignant spindle cell component (Fig. 1C) consistent with sarcomatoid differentiation. The tumor invaded the superficial muscularis propria (inner half) with metastatic carcinoma identified in one of 16 pelvic lymph nodes.

The postoperative course was complicated by hydronephrosis, pouchitis, and enteritis, and adjuvant chemotherapy was delayed. In April 2019, the patient started dose dense MVAC (methotrexate, vinblastine, doxorubicin, and Cisplatin) with granulocyte colony stimulating factor prophylaxis. She received two of four cycles and developed pseudomonas bacteremia and persistent liver function abnormalities attributed to chemotherapy. The patient was transitioned to Cisplatin and gemcitabine and within two cycles she developed new lower back pain in July 2019. CT of the abdomen and pelvis with contrast demonstrated new enhancing masses near the left pelvic sidewall and internal iliac vessels (reference mass, 3.4 × 2.8 cm; Fig. 2A). Biopsy of a pelvic mass confirmed sarcomatoid carcinoma with extensive necrosis that was histologically similar to the patient's bladder primary (Fig. 2C). Immunohistochemistry with the PDL-1 SP263 antibody revealed a combined positive score (CPS) of 100% (Fig. 2D).

Because of progression on cytotoxic chemotherapy, the patient was started on pembrolizumab 200 mg intravenously every 3 wk. After three cycles, response assessment on CT scan demonstrated decrease in size and enhancement of the left lower quadrant mass (2.3 × 1.5 cm) and associated lesions. After cycle 6, the CT scan revealed further reduction of the left lower quadrant mass (1.8 × 1.3 cm), consistent with overall 65% tumor burden decrease (partial response) (Fig. 2B).

To further characterize the genetic and pathologic characteristics of the patient's metastatic tumor, we performed NGS using a commercially available platform, PGDx elio tissue complete assay (Labriola et al. 2020) (Personal Genome Diagnostics, Inc.), 100 ng DNA input with 889× distinct coverage. No actionable single-nucleotide variants (SNVs) or translocations were detected. Microsatellite analysis showed that the tumor was microsatellite stable. The TMB was 10.8 mutations per megabase (Muts/Mb), predicted to be the exome equivalent of 3.1 (Muts/Mb). This is lower than the median of 5.5 somatic Muts/Mb in 130 urothelial carcinoma samples reported by the Cancer Genome Atlas Research Network (The Cancer Genome Atlas Research Network 2013). A low-fold *CD274* (PDL-1) amplification was detected in the metastatic tissue, but not in plasma cfDNA interrogated by PGDx elio plasma resolve assay (Al Zoughb et al. 2021). Blood collection occurred 2 wk after the biopsy,

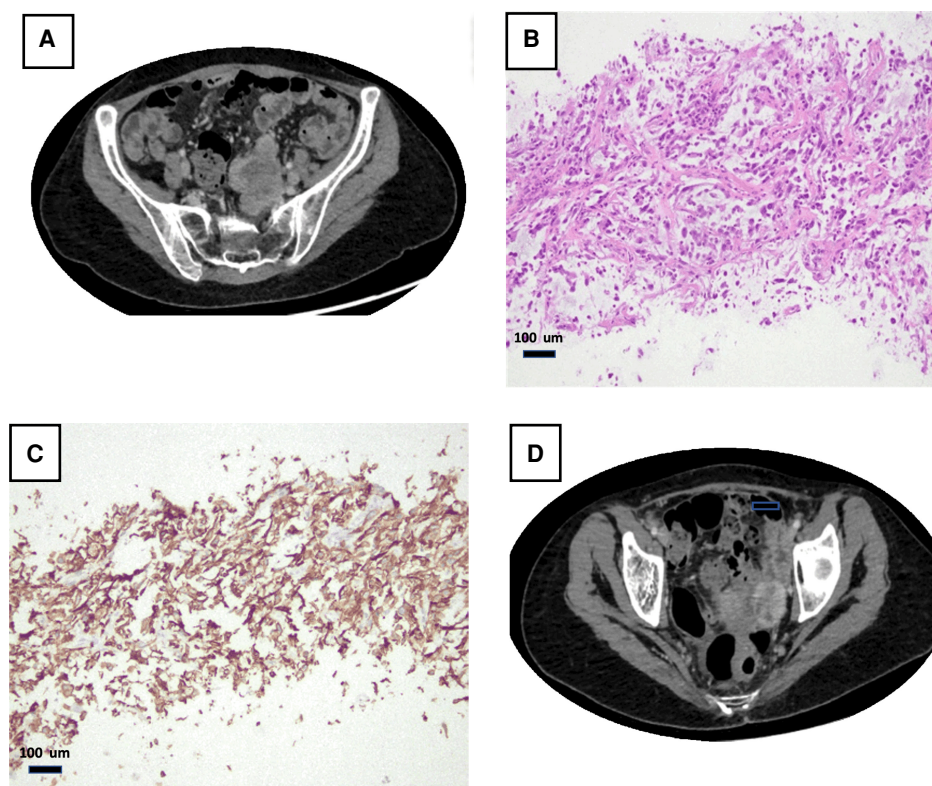


Figure 2. Clinicopathological presentation of metastatic sarcomatoid urothelial carcinoma (UC). Computed tomography (CT) with contrast showing an enhancing left pelvic mass (arrow) near the pelvic sidewall and near the left internal iliac vessels (A,B). Biopsy from that mass showed sarcomatoid carcinoma related to patient's known bladder primary (C). PDL-1 (SP263 antibody) shows a diffuse membranous staining, and the combined positive score (CPS) was 100% (D).

during which time the patient received the first cycle of pembrolizumab, which could explain the false-negative circulating free DNA (cfDNA) results.

Sequence mutation analysis in the metastatic tissue revealed variants in several cancer-related genes including oncogenes (*HRAS* and *GLI1*), tumor suppressor (*FAT1*), histone modifiers (*KDM6A*), and genes involved in various pathways (*CDKN1A*, cell cycle pathway; *KEAP1*, oxidative stress pathway). Mutations in the *TERT* promoter region and several other genes were detected (Tables 1 and 2). The G13P *HRAS* mutation was confirmed in the plasma and a F1101L *GLI1* mutation with high variant allele frequency (VAF) of 51% was detected. Although no germline confirmation was performed, such a *GLI1* variant was believed to represent a germline mutation given its high VAF. Based on VAF and the expected tumor purity (~18%), the *CDKN1A* and *KEAP1* mutations were suspected to represent a subclone of the original tumor. Plasma cfDNA sequencing confirmed G13P *HRAS* mutation (Tables 1 and 2).

To investigate the immune cell repertoire and PD-L1 expression in the SUC tumor cells and their immune microenvironment, we next performed IMC analysis of the metastatic tissue, capturing four areas of interest in the tissue covering 4.7 mm². We first observed the expression of tumoral (vimentin, pan-keratin) and immune markers (CD3, CD8a, CD4, CD20, CD68) in the tissue, particularly in the context of PD-L1 coexpression (Fig. 3A,B). To quantify the abundance of cell types, we detected cell boundaries in the images and quantified the

Table 1. PGDx elio tissue and plasma complete results

Gene	Source	Alteration	Mutation	MAF (%)	Role
CARD11	Tissue	T1022A	Missense	56.3	CARD-CC protein family costimulatory signal essential for T-cell receptor (TCR)-mediated T-cell activation
TLR4	Tissue	N176Ffs*27	Frameshift	38.8	Pathogen recognition and activation of innate immunity
CDKN1A	Tissue	W49S	Missense	5.9	Encodes cyclin-dependent kinase inhibitor
CDKN1A	Tissue	D52H	Missense	5.4	Cell cycle pathway
FAT1	Tissue	Y2774*	Nonsense	14.4	Tumor suppressor; cell proliferation
GLI1	Tissue	F1101L	Missense	51.0	Oncogene; Hedgehog signaling
HRAS	Tissue	G13P	Missense	17.5	Proto-oncogene
KDM6A	Tissue	K1018Efs*6	Frameshift	13.0	Histone demethylase: chromatin-modifying or chromatin-regulatory genes
KEAP1	Tissue	R272C	Missense	7.5	Tumor/metastasis suppressor; oxidative stress pathway
NCOR1	Tissue	H1401R	Missense	11.9	Histones/nuclear receptors
PTPRD	Tissue	N1701S	Missense	53.7	Unclear role
SLX4	Tissue	G1535E	Missense	48.3	DNA repair, DSBR HR
TERT	Tissue	n/a	Promoter	6.7	Telomerase complex
HRAS	Plasma	G13P	Missense	1.14	Proto-oncogene
HRAS	Plasma	n/a	Splice site Acceptor	0.54	Proto-oncogene

(MAF) Minor allele frequency, (DSBR) double-strand break repair, (HR) homologous recombination.

Table 2. Variant table

Gene	Genomic Location	Reference	Mutant	Amino acid change	Transcript	Consequence	MAF (%)
CARD11	Chr 7: 2951886–2951886	T	C	T1022A	CCDS5336.2	Missense	56.3
CDKN1A	Chr 6: 36652024–36652024	G	C	W49S	CCDS4824.1	Missense	5.9
CDKN1A	Chr 6: 36652032–36652032	G	C	D52H	CCDS4824.1	Missense	5.4
FAT1	Chr 4: 187539418–187539418	A	T	Y2774*	CCDS47177.1	Nonsense	14.4
GLI1	Chr 12: 57865824–57865824	T	C	F1101L	CCDS8940.1	Missense	51
HRAS	Chr 11: 534285–534286	CC	GG	G13P	NM_176795	Missense	17.5
KDM6A	Chr X:44938503–44938504	AA	n/a	K1018Efs*6	CCDS14265.1	Frameshift	13
KEAP1	Chr 19: 10602764–10602764	G	A	R272C	CCDS12239.1	Missense	7.5
NCOR1	Chr 17: 15973790–15973790	T	C	H1401R	CCDS11175.1	Missense	11.9
PTPRD	Chr 9: 8341114–8341114	T	C	N1701S	CCDS43786.1	Missense	53.7
SLX4	Chr 16: 3639035–3639035	C	T	G1535E	CCDS10506.2	Missense	48.3
TERT	Chr 5: 1295228–1295228	G	A	n/a	CCDS3861.2	Promoter	6.7
TLR4	Chr 9: 120474928–120474946	GACCAATCTA GAGCACTTG	n/a	N176Ffs*27	CCDS6818.1	Frameshift	38.8

(MAF) Minor allele frequency.

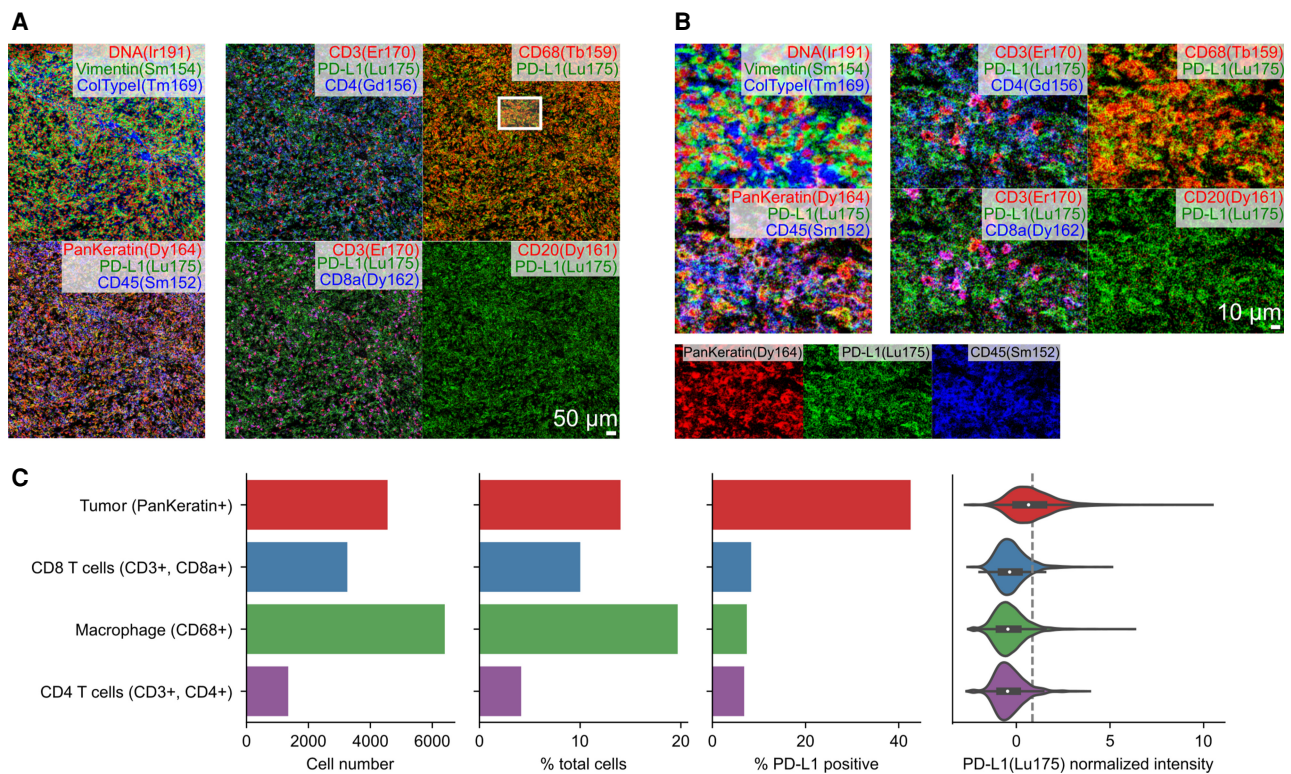


Figure 3. Tumor-immune microenvironment of metastatic sarcomatoid urothelial carcinoma (UC) revealed by Imaging Mass Cytometry. (A,B) Expression of PD-L1 in the context of coexpression of (A) tumor-specific or (B) immune-specific markers. (C) Quantification of cellular abundance in tumor and immune cells, and their expression of PD-L1.

intensity of these markers in each cell (Fig. 3C). We observed that macrophages were particularly abundant (20% of all cells), followed by tumor cells (14%). Intratumoral CD3 cells were also seen, with the majority being CD8a⁺ T cells (10% of total cells) and a smaller minority of CD4⁺ T cells (3% of total cells). PD-L1 expression was highest in pan-keratin-positive tumor cells (40% of PD-L1 positive cells) (Fig. 3C). PD-L1 expression was also seen at lower levels (5%–8%) in infiltrating CD68⁺ macrophages and CD4 and CD8 T-lymphocytes, which can help explain the immunohistochemical (IHC) findings (Fig. 3). Further characterization of cell type composition with PD-L1 expression, revealed five tumor cell groups (Fig. 4). One group of pan-keratin-positive tumor cells had high expression of PD-L1 and vimentin, but low expression of E-cadherin. A rarer group of tumor cells also had strong expression of PD-L1, along with CXCL12 and E-cadherin (Fig. 4).

Clinical Follow-Up to Date

The patient completed 30 cycles of pembrolizumab with no issues or new complains. The CT scan shows clean chest and stable abdominal disease.

DISCUSSION

UC has a propensity for divergent differentiation and the 2016 World Health Organization (WHO) classification of UCs lists 13 different histologic variants of urothelial cancer

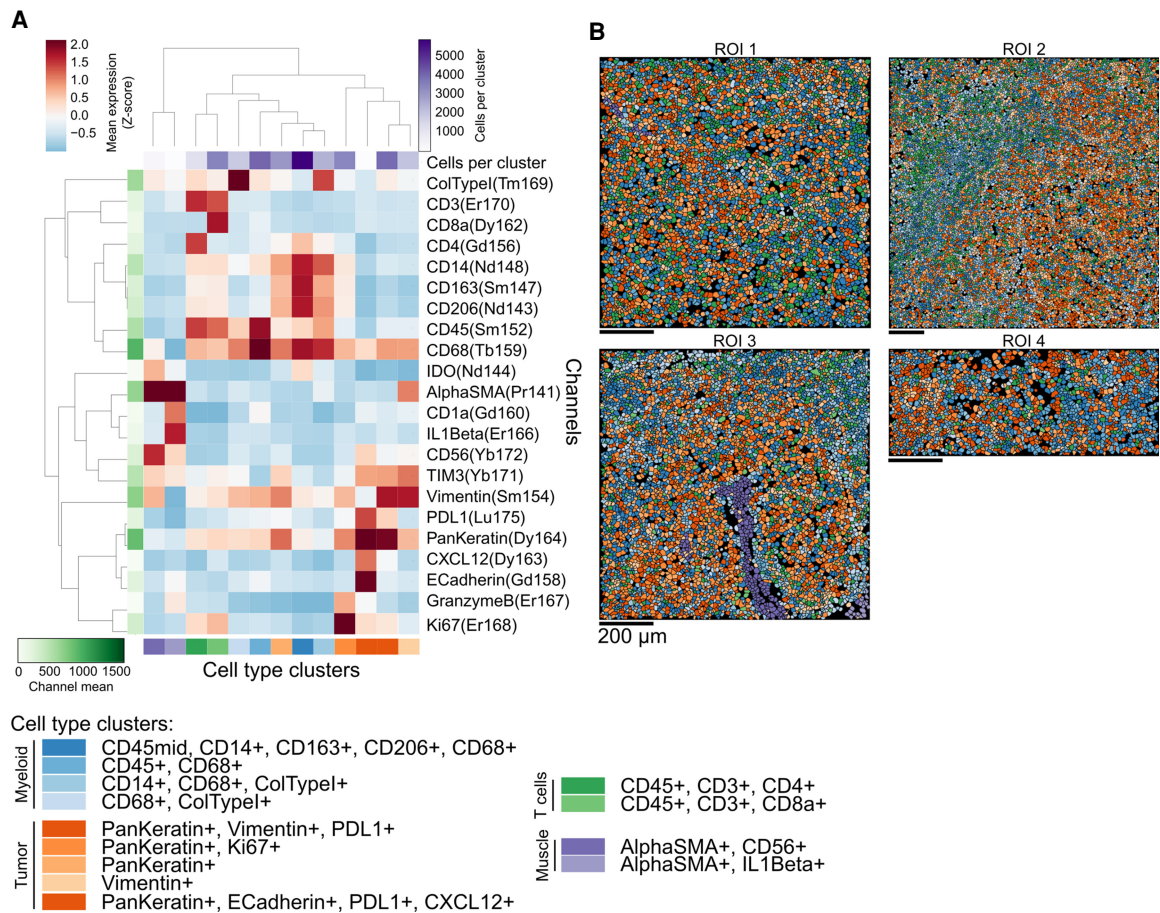


Figure 4. Molecular phenotype of tumor and immune cell repertoire of sarcomatoid urothelial carcinoma (UC). (A) Phenotype of discovered cellular clusters based on the profiles of marker expression as assessed by Imaging Mass Cytometry. Clusters are grouped by broad cell type ontogeny. (B) Representation of cells in the sarcomatoid carcinoma case in which each single cell is labeled with the color of the phenotypic cluster from A.

(Humphrey et al. 2016). However, there is a paucity of UC variants included in clinical trials resulting in low-level retrospective evidence for treatment recommendations.

SUCs show evidence of both epithelial and mesenchymal differentiation either histologically or by IHC and are believed to be the final common pathway for epithelial bladder tumors (Cheng et al. 2011). Sarcomatoid subtypes can also be seen in other tumor types. Reported data from sarcomatoid renal cell carcinoma (RCC) (Debien et al. 2020) and non-small-cell lung cancer (NSCLC) (Lou et al. 2016) show frequent expression of PD-L1 and high levels of tumor-infiltrating lymphocytes with an associated increased efficacy of PDL-1/PD-1 inhibition. Li et al. (2020) evaluated the PD-L1- and CD3-immune scores among invasive UC variants and found that cases of SUC demonstrate significantly higher PD-L1 scores as compared to conventional UC and other variants with high intratumoral CD3 scores.

IMC analysis in our case revealed similar patterns with a high number of infiltrating intratumoral CD3 cells, mainly CD8a⁺ T cells and with high PD-L1 expression in different cell types, mainly in pan-keratin-positive tumor cells. CD8a⁺ T cells are a crucial component of the cellular immune system that is important for cell-mediated antitumor immune response and independently associated with prolonged survival (Teng et al. 2015). PD-L1 expression

on different cellular populations (tumor cells and tumor infiltrating immune cells) might be associated with improved response to PD-1/PD-L1 inhibitors in UC patients (Wen et al. 2019) like our patient.

Tumors with epithelial-to-mesenchymal transition (EMT) have been shown to be associated with resistance to conventional therapy (Singh and Settleman 2010; Lou et al. 2016). EMT is a mechanism by which cancer cells can invade and metastasize by altering cellular properties such as epithelial cell–cell junctions, cytoskeletal organization, and tumor interactions with the microenvironment. Mak et al. (2016) observed a consistent and strong positive correlation between the EMT score and expression levels of immune checkpoint genes (including PD1, cytotoxic T-lymphocyte-associated protein 4, and tumor necrosis factor [TNF] receptor superfamily member 4), across all cancer types, including bladder cancer, with mesenchymal tumors expressing higher levels. Pathway analysis of those cases demonstrated enrichment of leukocyte extravasation signaling, suggesting immune activation. A study of 28 SUCs evaluating the expression of EMT markers showed that the majority of cases expressed pro-EMT transcriptional factors including FoxC2, SNAIL, and ZEB1, as well as vimentin, coupled with cadherin switching from E-cadherin to N-cadherin (Sanfrancesco et al. 2016). Although we did not evaluate N-cadherin, our case suggested that EMT may be at play, with the vast majority of tumor cells expressing vimentin and low E-cadherin expression. These same cells showed high expression of PD-L1. This is notable as the tumor demonstrated a rapid recurrence following surgical resection and resistance to cytotoxic chemotherapy while showing an excellent response to immunotherapy.

Goodman et al. (2018) studied the prevalence of *PD-L1* amplification in solid tumors, and amplifications were identified in 843 (0.7%) of the samples among more than 100 types of solid tumors. Most PD-L1-amplified tumors (84.8%) had a low (<5 Muts/Mb) to intermediate TMB (6–19 Muts/Mb), as in our case of low TMB (3.1 Muts/Mb). However, in contrast to our case, *PD-L1* amplification did not correlate with high-positive PD-L1 expression by immunohistochemical analysis in the same study (Goodman et al. 2018), emphasizing the need for better biomarkers. Six of nine patients (6/9; 66.7%) with PDL1-amplified solid tumors that were treated with immunotherapy had objective responses after checkpoint blockade administration, including one case of conventional UC (progression free survival of ≥ 17.8 mo). In another study, *PD-L1* amplification was more common in squamous cell carcinoma of the bladder and included only 17 cases (1%) of urothelial cancer (Necchi et al. 2020).

Conclusion

In conclusion, we present the first IMC analysis done in SUC to investigate the immune cell repertoire and PD-L1 expression on a single-cell level. The patient presented with metastatic SUC and experienced a prolonged response to the anti-PD1 immune checkpoint inhibitor pembrolizumab. Although the analysis on the metastatic tumor showed a low TMB, it demonstrated CD274 (PD-L1) amplification by NGS and 100% PD-L1 expression by IHC. IMC showed that most of the PD-L1 expression was present in tumor cells that showed evidence of EMT, as has been previously seen in SUC. The resistance of this tumor to conventional chemotherapy and sensitivity to immune checkpoint blockade suggests the importance of identifying genetic markers such as PD-L1 and others on a larger cohort of both UC and UC variants.

METHODS

This study was approved by the Institutional Review Board at Weill Cornell Medicine (Protocol # 1305013903—Research for Precision Medicine). Under this research protocol, patient provided written consent to be part of the study.

Tissue-Based NGS for Tumor Characterization

Protocols for DNA extraction and library preparation were followed, as previously described (Beg et al. 2021). NGS was performed by using the PGDx elio tissue complete RUO assay (Personal Genome Diagnostics, Inc.), a more than 500 gene panel targeted DNA-based assay that detects SNVs, small indels, translocations in 23 genes, amplifications in 28 genes, microsatellite instability, and TMB genomic signatures. The translocations detected by the assay are *ALK*, *AXL*, *BRAF*, *BRCA1*, *BRCA2*, *EGFR*, *ETV4*, *ETV6*, *EWSR1*, *FGFR1*, *FGFR2*, *FGFR3*, *MYC*, *NTRK1*, *NTRK2*, *NTRK3*, *PAX8*, *PDGFRA*, *PDGFRAB*, *RAF1*, *RET*, *ROS1*, and *TPR52* (Supplemental Fig. 1). Samples were processed as previously described (Labriola et al. 2020). Formalin-fixed, paraffin-embedded (FFPE) tumor tissue from this patient was evaluated by study pathologists. Sample processing from tissue, library preparation, hybrid capture, and sequencing were performed at the PGDx laboratory. Samples were run on the PGDx elio tissue complete tumor profiling NGS assay, screening for variants in the aforementioned genes. Briefly, DNA was extracted from FFPE tissue, and following shearing, genomic libraries were prepared using end repair, A tailing and adapter ligation modules. Genomic libraries were amplified and captured in-solution, targeting the predefined regions of interest across full exonic regions. Captured libraries were sequenced on an Illumina NextSeq platform (Supplemental Table S1).

Plasma-Based NGS for cfDNA Characterization

Protocols for blood fractionation, plasma cfDNA extraction, and library preparation were followed as previously described (Al Zoughbi et al. 2021). NGS was performed by using the PGDx elio plasma resolve RUO assay (Personal Genome Diagnostics, PGDx), an assay that interrogates full coding regions of 33 genes, copy-number variation of eight genes, five translocations, and microsatellite instability (MSI) (Supplemental Fig. 2).

Antibody Panel Design and Validation for IMC

Preconjugated metal labeled antibodies were bought from Fluidigm, which were tested for specificity according to the company datasheet. The rest of the antibodies were custom-conjugated following manufacturer's protocol using the Maxpar X8 Multimetal Labeling Kit (Maxpar 201300). Newly conjugated antibodies were tested for staining specificity by staining control tissues such as lymph node. The PD-L1 clone SP142 was chosen based on its staining pattern that was close enough to the IHC clone used for scoring. A pathologist verifies the staining pattern for all antibodies before proceeding with actual staining of the tissue.

Imaging Mass Cytometry

Based on the clinical and pathological characteristics and quality of the preserved tissues, suitable representative fresh-cut 4- μ m-thick FFPE sections were used for IMC staining. Slides were incubated for 1 h at 60°C on a slide warmer followed by dewaxing in fresh CitriSolv (Decon Labs) twice for 10 min, rehydrated in descending series of 100%, 95%, 80%, and 75% ethanol for 5 min each. After 5 min of MilliQ water wash, the slides were treated with antigen retrieval solution (Tris-EDTA pH 9.2) for 30 min at 96°C. Slides were cooled to room temperature, washed twice in TBS, and blocked for 1.5 h in SuperBlock Solution (Thermo Fisher), followed by overnight incubation at 4°C with the prepared antibody cocktail containing all metal-labeled antibodies (Table 3). The next day, slides were washed twice in 0.2% Triton X-100 in PBS and twice in TBS. DNA staining was performed using Intercalator-Iridium in PBS solution for 30 min in a humid chamber at room temperature. Slides were washed with MilliQ water and air-dried before ablation.

Table 3. Full list of antibodies and their properties

Antibody	Metal tag	Clone	Dilution	Stock concentration (mg/mL)	Vendor	Catalog #
Alpha-smooth muscle actin	Pr141	1A4	1:400	0.5	Fluidigm	3141017D
Interferon gamma	Nd142	IFNG/466	1:50	0.5	Abcam	ab218890
CD206	Nd143	E2L9N	1:100	0.2	Cell Signaling Technology	91992BF
IDO	Nd144	D5J4E	1:50	0.5	Cell Signaling Technology	86630BF
LAG3	Nd145	D2G40	1:50	0.5	Cell Signaling Technology	15372BF
CD163	Sm147	EDHu-1	1:100	0.5	Fluidigm	3147021D
CD14	Nd148	D7A2T	1:50	0.5	Cell Signaling Technology	56082BF
PD1	Nd150	D4W2J	1:50	0.5	Cell Signaling Technology	86163BF
CD45	Sm152	D9M8I	1:100	0.5	Fluidigm	3152018D
CD44	Eu153	IM7	1:100	0.5	BioLegend	103001
Vimentin	Sm154	D21H3	1:200	0.5	Fluidigm	3154014A
FoxP3	Gd155	236A/E7	1:25	0.5	Abcam	ab96048
CD4	Gd156	OT15D9	1:50	0.5	Novus Biologicals	NBP2-70357
E-cadherin	Gd158	2.40E + 11	1:100	0.5	Fluidigm	3158029D
CD68	Tb159	KP1	1:50	0.5	Abcam	ab233172
CD1a	Gd160	O10	1:50	0.5	Abcam	ab212980
CD20	Dy161	L26	1:200	0.5	Novus Biologicals	NBP2-80486
CD8a	Dy162	C8/144B	1:100	0.5	eBioscience	14-0085-82
CXCL12	Dy163	D7A2T	1:50	0.5	Abcam	97958BF
Pan-keratin	Dy164	AE1/AE3	1:100	0.5	Abcam	ab80826
HLADR	Ho165	EPR3692	1:50	0.5	Abcam	ab215985
IL-1beta	Er166	3A6	1:50	0.5	Cell Signaling Technology	12242BF
Granzyme B	Er167	GB11	1:50	0.5	Fluidigm	3167023D
Ki67	Er168	B56	1:50	0.5	Fluidigm	3168022D
ColTypeI	Tm169	Polyclonal	1:300	0.5	Fluidigm	3169023D
CD3	Er170	Polyclonal, carboxy-terminal	1:100	0.5	Fluidigm	3170019D
TIM3	Yb171	D5D5R	1:50	0.5	Cell Signaling Technology	45208BF
CD56	Yb172	3H15L12	1:50	0.5	Invitrogen	701379
CD45RO	Yb173	UCHL1	1:100	0.5	Fluidigm	3173016D
HLAclassI	Yb174	EMR8-5	1:50	0.5	Abcam	ab70328
PDL1	Lu175	SP142	1:50	0.5	Abcam	ab236238
CD11c	Yb176	EP1347Y	1:50	0.5	Abcam	ab216655
DNA1	Ir191		1:400		Fluidigm	201192A
DNA2	Ir193		1:400		Fluidigm	201192A

The instrument was calibrated using a tuning slide to optimize the sensitivity of the detection range. Hematoxylin and eosin–stained slides were used to guide the selection of four regions of interest based on the pathological examination of the tissue. Scanning protocol was set for 200 Hz frequency and the raw MCD file was exported for downstream data analysis.

Preprocessing of IMC Data

IMC data was preprocessed as described previously (Zanotelli and Bodenmiller 2017), with some modifications. Briefly, image data was extracted from MCD files acquired with the Fluidigm Hyperion instrument. Hot pixels were removed using a fixed threshold, the image was amplified two times, and Gaussian smoothing applied. From each image a square 500-pixel crop was saved as a HDF5 file for image segmentation.

Image segmentation was performed with ilastik (Berg et al. 2019) (version 1.3.3) by manually labeling pixels as belonging to one of three classes: nuclei; cytoplasm—as the area immediately surrounding the nuclei; and background—as pixels with low signal across all channels. Output probabilities were used to segment the image using CellProfiler (Carpenter et al. 2006) (version 3.1.8) with the IdentifyPrimaryObjects module, and followed by the “IdentifySecondaryObjects” module in which identified nuclei are used to seed an expansion of the cell area to generate a cellular mask.

Analysis of IMC Data

We assessed the quality of each acquired channel as described previously (Rendeiro et al. 2021) and quantified single cells by averaging signal intensity of each channel in the area of each cell in the cell mask. We used Scanpy (Wolf et al. 2018) (version 1.5.0) to process the single-cell data. Values were log_{1p} transformed and normalized in order for the sum of each cell to equal 1×10^4 . Cell type assignment was performed by computing a neighbor graph on this standardized and centered matrix with eight neighbors per cell and by clustering the cells with the Leiden algorithm (Traag et al. 2019) in the Python implementation (leidenalg, version 0.8.0), with 0.75 as resolution parameter. To derive data-driven labels for each cluster, we used the mean intensity of each cluster in each channel, centered and scaled in both dimensions, averaged for both (Wisconsin double transformation). To those values, we fit a Gaussian Mixture model (scikit-learn, version 0.23.0) with two classes and used the decision boundary to label each cluster above that value as positive for that marker. The union of positive markers for a given cluster was used as a label for the cluster. To declare cells as positive for a certain marker, we also used a Gaussian mixture model with two classes except the ones run for each marker using the log-transformed intensity matrix.

The following additional software versions were used: Python version 3.8.2, numpy version 1.18.3, scipy version 1.4.1, and scikit-image 0.17.2.

ADDITIONAL INFORMATION

Data Deposition and Access

IMC data can be found at the following publicly accessible repository: <https://doi.org/10.5281/zenodo.6251220>. Source code used to analyze IMC data are available at <https://github.com/ElementoLab/msuc-imc>. Additional data that support the findings of this study are available on request from the corresponding author (J.M.M.). Interpreted variants were submitted to ClinVar (<https://www.ncbi.nlm.nih.gov/clinvar/>) and can be found under accession numbers SCV002500974–SCV002500987.

Ethics Statement

This study was approved by the Institutional Review Board (Protocol # 1305013903). Written informed consent was obtained from the patient for publication of this case report and any accompanying images.

Acknowledgments

We thank Christen Vinson and Leandra Slayton from Personal Genome Diagnostics, Inc. for their significant discussion of the manuscript.

Author Contributions

J.M.M. devised the project, the main conceptual ideas and proof outline. H.R. performed IMC experiments. A.F.R. analyzed IMC data. H.A. wrote the manuscript with input from all authors. All authors discussed the results and commented on the manuscript.

Competing Interest Statement

J.M.M. had a research collaboration agreement with Personal Genome Diagnostics Inc. during 2019–2020.

Received September 1, 2021;
accepted in revised form
March 3, 2022.

Funding

This work was supported by the Caryl and Israel Englander Institute for Precision Medicine. A.F.R. is supported by a T32 grant from the National Cancer Institute. This work was supported in part by the Cornell Center for Immunology Core Facilities Seed Grant (Principal Investigator, J.M.M.; Co-Principal Investigator, K.O.; and Co-Investigators, O.E. and B.F.).

REFERENCES

- Al Zoughbi W, Fox J, Beg SB, Papp E, Hissong E, Ohara K, Keefer L, Sigouros M, Kane T, Bockelman D, et al. 2021. Validation of a ctDNA-based next-generation sequencing assay in a cohort of solid tumor patients: a proposed solution for decentralized plasma testing. *Oncologist* **26**: e1971–e1981. doi:10.1002/onco.13905
- Beg S, Bareja R, Ohara K, Eng KW, Wilkes DC, Pisapia DJ, Al Zoughbi W, Kudman S, Zhang W, Rao R, et al. 2021. Integration of whole-exome and anchored PCR-based next generation sequencing significantly increases detection of actionable alterations in precision oncology. *Transl Oncol* **14**: 1. doi:10.1016/j.tranon.2020.100944
- Berg S, Kutra D, Kroeger T, Straehle CN, Kausler BX, Haubold C, Schiegg M, Ales J, Beier T, Rudy M, et al. 2019. ilastik: interactive machine learning for (bio)image analysis. *Nat Methods* **16**: 1226–1232. doi:10.1038/s41592-019-0582-9
- Carpenter AE, Jones TR, Lamprecht MR, Clarke C, Kang IH, Friman O, Guertin DA, Chang JH, Lindquist RA, Moffat J, et al. 2006. CellProfiler: image analysis software for identifying and quantifying cell phenotypes. *Genome Biol* **7**: R100. doi:10.1186/gb-2006-7-10-r100
- Cheng L, Zhang S, Alexander R, MacLennan GT, Hodges KB, Harrison BT, Lopez-Beltran A, Montironi R. 2011. Sarcomatoid carcinoma of the urinary bladder: the final common pathway of urothelial carcinoma dedifferentiation. *Am J Surg Pathol* **35**: e34–e36. doi:10.1097/PAS.0b013e3182159dec
- Debien V, Thouvenin J, Lindner V, Barthélémy P, Lang H, Flippot R, Malouf GG. 2020. Sarcomatoid dedifferentiation in renal cell carcinoma: from novel molecular insights to new clinical opportunities. *Cancers (Basel)* **12**: 99. doi:10.3390/cancers12010099
- De Santis M, Bellmunt J, Mead G, Kerst JM, Leahy M, Maroto P, Gil T, Marreaud S, Daugaard G, Skoneczna I, et al. 2012. Randomized phase II/III trial assessing gemcitabine/carboplatin and methotrexate/carboplatin/vinblastine in patients with advanced urothelial cancer who are unfit for cisplatin-based chemotherapy: eORTC study 30986. *J Clin Oncol* **30**: 191–199. doi:10.1200/JCO.2011.37.3571
- Fradet Y, Bellmunt J, Vaughn DJ, Lee JL, Fong L, Vogelzang NJ, Climent MA, Petrylak DP, Choueiri TK, Necchi A, et al. 2019. Randomized phase III KEYNOTE-045 trial of pembrolizumab versus paclitaxel, docetaxel, or vinflunine in recurrent advanced urothelial cancer: results of >2 years of follow-up. *Ann Oncol* **30**: 970–976. doi:10.1093/ANNONC/MDZ127
- Gakis G. 2014. The role of inflammation in bladder cancer. *Adv Exp Med Biol* **816**: 183–196. doi:10.1007/978-3-0348-0837-8_8
- Giesen C, Wang HA, Schapiro D, Zivanovic N, Jacobs A, Hattendorf B, Schüffler PJ, Grolimund D, Buhmann JM, Brandt S, et al. 2014. Highly multiplexed imaging of tumor tissues with subcellular resolution by mass cytometry. *Nat Methods* **11**: 417–422. doi:10.1038/NMETH.2869
- Goodman AM, Piccioni D, Kato S, Boichard A, Wang HY, Frampton G, Lippman SM, Connelly C, Fabrizio D, Miller V, et al. 2018. Prevalence of PDL1 amplification and preliminary response to immune checkpoint blockade in solid tumors. *JAMA Oncol* **4**: 1237–1244. doi:10.1001/jamaoncol.2018.1701
- Grossman HB, Natale RB, Tangen CM, Speights VO, Vogelzang NJ, Trump DL, deVere White RW, Sarosdy MF, Wood DP, Raghavan D, et al. 2003. Neoadjuvant chemotherapy plus cystectomy compared with

- cystectomy alone for locally advanced bladder cancer. *N Engl J Med* **349**: 859–866. doi:10.1056/NEJMoa022148
- Humphrey PA, Moch H, Cubilla AL, Ulbright TM, Reuter VE. 2016. The 2016 WHO classification of tumours of the urinary system and male genital organs—part B: prostate and bladder tumours. *Eur Urol* **70**: 106–119. doi:10.1016/j.eururo.2016.02.028
- Labriola MK, Zhu J, Gupta R, McCall S, Jackson J, Kong EF, White JR, Cerqueira G, Gerding K, Simmons JK, et al. 2020. Characterization of tumor mutation burden, PD-L1 and DNA repair genes to assess relationship to immune checkpoint inhibitors response in metastatic renal cell carcinoma. *J Immunother Cancer* **8**: e000319. doi:10.1136/jitc-2019-000319
- Li H, Zhang Q, Shuman L, Kaag M, Raman JD, Merrill S, DeGraff DJ, Warrick JI, Chen G. 2020. Evaluation of PD-L1 and other immune markers in bladder urothelial carcinoma stratified by histologic variants and molecular subtypes. *Sci Rep* **10**: 1439. doi:10.1038/s41598-020-58351-6
- Lou Y, Diao L, Cuentas ERP, Denning WL, Chen L, Fan YH, Byers LA, Wang J, Papadimitrakopoulou VA, Behrens C, et al. 2016. Epithelial-mesenchymal transition is associated with a distinct tumor microenvironment including elevation of inflammatory signals and multiple immune checkpoints in lung adenocarcinoma. *Clin Cancer Res* **22**: 3630–3642. doi:10.1158/1078-0432.CCR-15-1434
- Mak MP, Tong P, Diao L, Cardnell RJ, Gibbons DL, William WN, Skouldis F, Parra ER, Rodriguez-Canales J, Wistuba II, et al. 2016. A patient-derived, pan-cancer EMT signature identifies global molecular alterations and immune target enrichment following epithelial-to-mesenchymal transition. *Clin Cancer Res* **22**: 609–620. doi:10.1158/1078-0432.CCR-15-0876
- Nakanishi J, Wada Y, Matsumoto K, Azuma M, Kikuchi K, Ueda S. 2007. Overexpression of B7-H1 (PD-L1) significantly associates with tumor grade and postoperative prognosis in human urothelial cancers. *Cancer Immunol Immunother* **56**: 1173–1182. doi:10.1007/s00262-006-0266-z
- Necchi A, Madison R, Raggi D, Jacob JM, Bratslavsky G, Shapiro O, Elvin JA, Vergilio JA, Killian JK, Ngo N, et al. 2020. Comprehensive assessment of immuno-oncology biomarkers in adenocarcinoma, urothelial carcinoma, and squamous-cell carcinoma of the bladder. *Eur Urol* **77**: 548–556. doi:10.1016/j.eururo.2020.01.003
- Powles T, Park SH, Voog E, Caserta C, Valderrama BP, Gurney H, Kalofonos H, Radulovic S, Demey W, Ullén A, et al. 2020. Maintenance avelumab + best supportive care (BSC) versus BSC alone after platinum-based first-line (1L) chemotherapy in advanced urothelial carcinoma (UC): JAVELIN Bladder 100 phase III interim analysis. *J Clin Oncol* **38**: LBA1. doi:10.1200/jco.2020.38.18_suppl.lba1
- Rendeiro AF, Ravichandran H, Bram Y, Chandar V, Kim J, Meydan C, Park J, Foox J, Hether T, Warren S, et al. 2021. The spatial landscape of lung pathology during COVID-19 progression. *Nature* **593**: 564–569. doi:10.1038/s41586-021-03475-6
- Sanfrancesco J, McKenney JK, Leivo MZ, Gupta S, Elson P, Hansel DE. 2016. Sarcomatoid urothelial carcinoma of the bladder: analysis of 28 cases with emphasis on clinicopathologic features and markers of epithelial-to-mesenchymal transition. *Arch Pathol Lab Med* **140**: 543–551. doi:10.5858/arpa.2015-0085-OA
- Singh A, Settleman J. 2010. EMT, cancer stem cells and drug resistance: an emerging axis of evil in the war on cancer. *Oncogene* **29**: 4741–4751. doi:10.1038/onc.2010.215
- Sternberg CN, De Mulder P, Schornagel JH, Theodore C, Fossa SD, Van Oosterom AT, Witjes JA, Spina M, Van Groeningen CJ, Duclos B, et al. 2006. Seven year update of an EORTC phase III trial of high-dose intensity M-VAC chemotherapy and G-CSF versus classic M-VAC in advanced urothelial tract tumours. *Eur J Cancer* **42**: 50–54. doi:10.1016/j.ejca.2005.08.032
- Teng MWL, Ngiew SF, Ribas A, Smyth MJ. 2015. Classifying cancers based on T-cell infiltration and PD-L1. *Cancer Res* **75**: 2139–2145. doi:10.1158/0008-5472.CAN-15-0255
- The Cancer Genome Atlas Research Network. 2013. Comprehensive molecular characterization of urothelial bladder carcinoma: The Cancer Genome Atlas Research Network. *Nature* **507**: 315–322. doi:10.1038/nature12965
- Traag VA, Waltman L, van Eck NJ. 2019. From Louvain to Leiden: guaranteeing well-connected communities. *Sci Rep* **9**: 5233. doi:10.1038/s41598-019-41695-z
- Tripathi A, Plimack ER. 2018. Immunotherapy for urothelial carcinoma: current evidence and future directions. *Curr Urol Rep* **19**: 109. doi:10.1007/s11934-018-0851-7
- Wang J, Wang FW, Lagrange CA, Hemstreet GP Iii, Kessinger A. 2010. Clinical features of sarcomatoid carcinoma (carcinosarcoma) of the urinary bladder: analysis of 221 cases. *Sarcoma* **2010**: 454792. doi:10.1155/2010/454792
- Wen Y, Chen Y, Duan X, Zhu W, Cai C, Deng T, Zeng G. 2019. The clinicopathological and prognostic value of PD-L1 in urothelial carcinoma: a meta-analysis. *Clin Exp Med* **19**: 407–416. doi:10.1007/s10238-019-00572-9
- Wolf FA, Angerer P, Theis FJ. 2018. SCANPY: large-scale single-cell gene expression data analysis. *Genome Biol* **19**: 15. doi:10.1186/s13059-017-1382-0

Wright JL, Black PC, Brown GA, Porter MP, Kamat AM, Dinney CP, Lin DW. 2007. Differences in survival among patients with sarcomatoid carcinoma, carcinosarcoma and urothelial carcinoma of the bladder. *J Urol* **178**: 2302–2307. doi:10.1016/j.juro.2007.08.038

Zanotelli VRT, Bodenmiller B. 2017. *ImcSegmentationPipeline: a pixelclassification based multiplexed image segmentation pipeline*. doi:10.5281/ZENODO.3841961